heating. The net result of the competing processes is the decrease in the local heat-transfer coefficient with time. Steady state natural convection heat transfer from a vertical plate suspended in an infinite volume of liquid predicted by boundary-layer theory [8],

$$Nu_x/Ra_x^{1/4} = 0.503[1 + (0.492/Pr)^{9/6}]^{-4/9} \quad (3)$$

is included for the purpose of comparison. The predictions are seen to bound natural convection heat-transfer data in the presence of phase change and recirculation.

The largest heat-transfer coefficients along the solid–liquid interface occur near the top of the test cell where there is a 90° turn in the flow direction. The presentation of results in dimensionless form ($Nu_x/Ra_x^{1/4}$) also reveals this maximum. With continued heating and changing natural circulation flow in the melt region, the maximum moves down along the solid–liquid interface.

The effect of Stefan number on the heat-transfer coefficient at the heat surface and at the solid–liquid interface are presented in Figs. 3(a) and 3(b), respectively. Results could not be obtained for the lower part of the heated surface because the interferometer optics were too small to accommodate the entire cell. For comparison purposes, results are also included in Fig. 3(a) for transient natural convection heat transfer from a vertical surface in the absence of phase change. At this time (t = 45 min) quasi-steady natural convection appears to have been established, but because of thermal stratification in a finite-size test cell the heat-transfer parameter $Nu_x/Ra_x^{1/4}$ was not constant but decreased with the distance along the heated surface. At a given time, the heat-transfer coefficients at both the heated surface and the interface are seen to be lower for the higher Stefan numbers. This is attributed to a simultaneous occurrence of two main effects: (1) alteration of the natural convection flow field due to the change in size and shape of the melt region, and (2) modification of the temperature distribution. These changes are clearly seen in the interferograms presented in Fig. 1.

A meaningful comparison of the heat-transfer results ($Nu_x/Ra_x^{1/4}$) at the solid–liquid interface reported by Hale and Viskanta [3] with those of this work could not be made because of large differences in the Stefan and Rayleigh numbers as well as the hydrodynamic conditions at the top of the test cell. The results are in the range of those given in Fig. 3 (b).

The interferometer has provided detailed information about the heat transfer processes taking place at the heated surface and the interface which has not been reported in the literature previously, but the instrument is not without its limitations. The drawback of the interferometer is that at early times the melt layer is not sufficiently thick to permit the passage of enough light to produce sharp interference fringes. Consequently, temperature distribution data could not be obtained at early times when heat transfer by conduction predominated and/or natural convection was just beginning to develop because the melt layer was too thin. In addition, the index of refraction of n-heptadecane is very sensitive to temperature, and therefore only small superheats ($T_w - T_f$) could be used in the experiments to permit interpretation of the interferograms because of too large fringe density. The exploratory results reported in this note suggest that several additional effects and parameters must be considered in correlating natural convection heat transfer results during solid-to-liquid phase change in a finite-melt region.

Acknowledgements – This work was supported by the National Science Foundation Heat Transfer Program under Grant No. ENG-7811686.

REFERENCES

1. R. H. Turner, *High Temperature Energy Thermal Storage*. Franklin Institute Press, Philadelphia, 1978.
2. J. W. Ramsey and E. M. Sparrow, Melting and natural convection due to a vertical embedded heater, *J. Heat Transfer* **100C**, 368–370 (1978).
3. N. W. Hale, Jr. and R. Viskanta, Photographic observation of the solid–liquid interface motion during melting of a solid heat from an isothermal vertical wall, *Letters Heat Mass Transfer* **5**, 329–337 (1978).
4. E. M. Sparrow, S. V. Patankar and S. Ramadhyani, Analysis of melting in the presence of natural convection in the melt region, *J. Heat Transfer* **99C**, 520–526 (1977).
5. R. H. Marshall, Natural convection effects in rectangular enclosures containing a phase change material, in *Thermal Storage and Heat Transfer in Solar Energy Systems*, edited by F. Kreith *et al.* pp. 61–69. ASME, New York (1978).
6. W. Hauf and W. Grigull, Optical methods in heat transfer, in *Advances in Heat Transfer*, edited by T. F. Irvine, Jr. and J. P. Hartnett, Vol. 6, pp. 133–366. Academic Press, New York (1970).
7. J. D. Hellums and S. W. Churchill, Transient and steady state, free and natural convection numerical solutions—I. The isothermal, vertical plate, *A.I.Ch.E. Jl* **8**, 690–692 (1962).
8. S. W. Churchill and H. Ozoe, A correlation for laminar free convection from a vertical plate, *J. Heat Transfer* **95C**, 540–541 (1973).

Int. J. Heat Mass Transfer. Vol. 23, pp. 571–576

0017-9310/80/0401-0571 $02.00/0

MEASUREMENTS AND CALCULATIONS OF TRANSIENT NATURAL CONVECTION IN AIR

B. SAMMAKIA, B. GEBHART and Z. H. QURESHI
Department of Mechanical Engineering, State University of New York at Buffalo, Amherst, NY 14260, U.S.A.

(*Received* 16 *May* 1979 *and in revised form* 21 *August* 1979)

NOMENCLATURE

c_p, fluid specific heat;
c'', thermal capacity of element per unit surface area;
g, gravitational acceleration [m/s²];
G^*, $5\left[\frac{Gr_x^*}{5}\right]^{1/5}$;
Gr^*, non-dimensional modified Grashof number, $\frac{g\beta q'' x^4}{kv^2}$;
h, heat-transfer coefficient;
k, thermal conductivity [W/mK];
Pr, Prandtl number;

q'', instantaneous energy generation rate per unit of element surface area [W/m^2];
Q^*, thermal capacity parameter related to the element storage; capacity, $c''\left[\frac{g\beta q'' v^2}{k^5}\right]^{1/4}$;
s, half the thickness of the plate;
t, static temperature [K];
t_0, instantaneous local plate temperature [K];
t_∞, temperature of the undisturbed fluid [K];
T, non-dimensional temperature, $\frac{(t-t_\infty)}{(v^2q''^3/g\beta k^3)^{1/4}}$;
u, component of velocity in vertical direction;
U, non-dimensional velocity, $\frac{u}{(v^2g\beta q''/k)^{1/4}}$;
v, component of velocity in horizontal direction;
V, non-dimensional velocity, $\frac{v}{(v^2g\beta q''/k)^{1/4}}$;
x, vertical distance above bottom of plate;
X, non-dimensional vertical distance, $\frac{x}{(v^2k/g\beta q'')^{1/4}}$;
y, horizontal distance from plate;
Y, non-dimensional horizontal distance, $\frac{y}{(v^2k/g\beta q'')^{1/4}}$.

Greek symbols

α, thermal diffusivity of fluid;
β, coefficient of thermal expansion of fluid;
σ, Stefan Boltzman constant;
ν, kinematic viscosity [m^2/s];
ρ, density of fluid;
ε, surface emissivity;
$\bar{\tau}$, time;
τ, non-dimensional time, $\frac{\bar{\tau}}{(k/g\beta q'')^{1/2}}$.

Subscripts

0, at solid–fluid interface;
ss, steady state;
∞, free stream conditions;
BT, beginning of transition;
ET, end of transition.

INTRODUCTION

A PREVIOUS paper [1] presented numerical solutions for natural convection transients generated adjacent to flat vertical plates, in quiescent air. Relevant previous literature concerning transient response was reviewed there. Comparisons were made between the new results and both theoretical and experimental results. Those calculations were given for a wide range of plate thermal capacity for a step in energy input to the element. The calculations were for a Prandtl number = 0.72. No radiation effect was considered at the surface. Three different regimes of transients were shown to occur.

This paper presents the results of much more detailed measurements of natural convection transients adjacent to a flat vertical plate in air. The effect of thermal radiation from the surface is included and accounted for in the boundary conditions. The nondimensional governing equations embodying the boundary layer and Boussinesq approximations, which were used in the calculations, are

$$\frac{\partial U}{\partial X}+\frac{\partial V}{\partial Y}=0 \tag{1}$$

$$\frac{\partial U}{\partial \tau}+U\frac{\partial U}{\partial X}+V\frac{\partial U}{\partial Y}=T+\frac{\partial^2 U}{\partial Y^2} \tag{2}$$

$$\frac{\partial T}{\partial \tau}+U\frac{\partial T}{\partial X}+V\frac{\partial T}{\partial Y}=\frac{1}{Pr}\frac{\partial^2 T}{\partial Y^2} \tag{3}$$

where

$$T=\frac{t-t_\infty}{(v^2q''^3/g\beta k^3)^{1/4}} \qquad \tau=\frac{\bar{\tau}}{(k/g\beta q'')^{1/2}}$$

$$U=\frac{u}{(v^2g\beta q''/k)^{1/4}} \qquad V=\frac{v}{(v^2g\beta q''/k)^{1/4}}$$

$$X=\frac{x}{(v^2k/g\beta q'')^{1/4}}=(Gr_x^*)^{1/4}$$

$$Y=\frac{y}{(v^2k/g\beta q'')^{1/4}}=(Gr_x^*)^{1/4}\frac{y}{x}.$$

The corresponding boundary and initial conditions are

$$\tau=0 \quad U=V=T=0 \tag{4}$$

$$X=0 \quad U=V=T=0 \tag{5}$$

$$Y=0 \quad U=V=0 \tag{6}$$

$$Y\to\infty \quad U=V=T=0 \tag{7}$$

$Y=0$

$$1=Q^*\left(\frac{\partial T}{\partial \tau}\right)_0-\left(\frac{\partial T}{\partial Y}\right)_0+\left(\frac{\sigma\varepsilon}{q''}\right)(t_0^4-t_\infty^4) \tag{8}$$

where equation (8) is the result of an energy balance on the plate. Calculations over a wide range of Q^* are presented in [1]. The last term in equation (8) is added here to account for thermal radiation from the plate surface. It may be an appreciable effect in air, even with a surface of low emissivity.

NUMERICAL CALCULATIONS

The same numerical technique is used as in [1], namely an explicit finite difference scheme. To reduce the radiation term to an appropriate non-dimensional form, the following approximation is made

$$t_0^4-t_\infty^4=A+B(t_0-t_\infty)+C(t_0-t_\infty)^2+D(t_0-t_\infty)^3+E(t_0-t_\infty)^4$$

where the constants A, B, C, D and E are evaluated as the coefficients of a fourth order polynomial. Thus, equation (8) reduces to

$$1=Q^*\left(\frac{\partial T}{\partial \tau}\right)_0-\left(\frac{\partial T}{\partial Y}\right)_0+\frac{\sigma\varepsilon}{q''}\times[A+BRT_0+CR^2T_0^2+DR^3T_0^3+ER^4T_0^4]$$

where

$$R=\left(\frac{v^2q''^3}{g\beta k^3}\right)^{1/4}$$

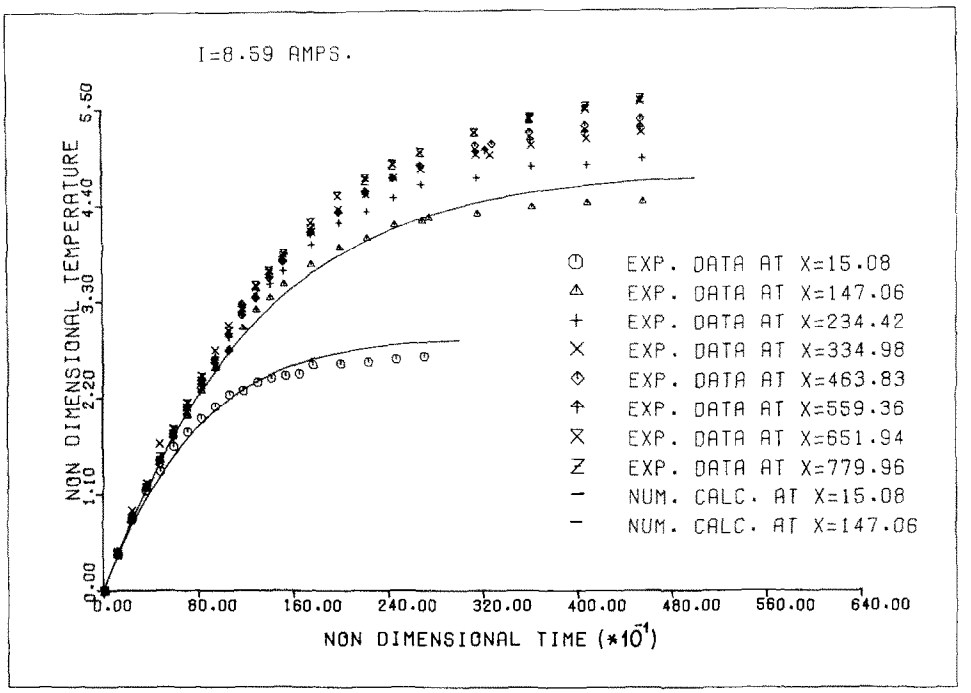

FIG. 1. Comparison of measured surface temperature response to finite difference calculations.

The air properties are calculated at the film temperature where $t_{film} = (t_0 + t_\infty)/2$. To minimize the error due to the leading edge effect each x-location is considered to be the top of a plate, and calculations are carried out separately for that location. The grid spacing is kept constant, i.e. m and n are varied to keep ΔX and ΔY approximately constant where $\Delta X = X_{max}/m$, $\Delta Y = Y_{max}/n$.

APPARATUS

A flat vertical plate was instantaneously loaded with thereafter uniform and constant input heat flux. This generates a buoyancy induced flow in the adjacent air. The surface assembly consists of two Inconnel 600 foils, 0.00127 cm thick, 130.5 cm long and 46.6 cm wide. These were separated by layers of Teflon and glass fabric. The thermal

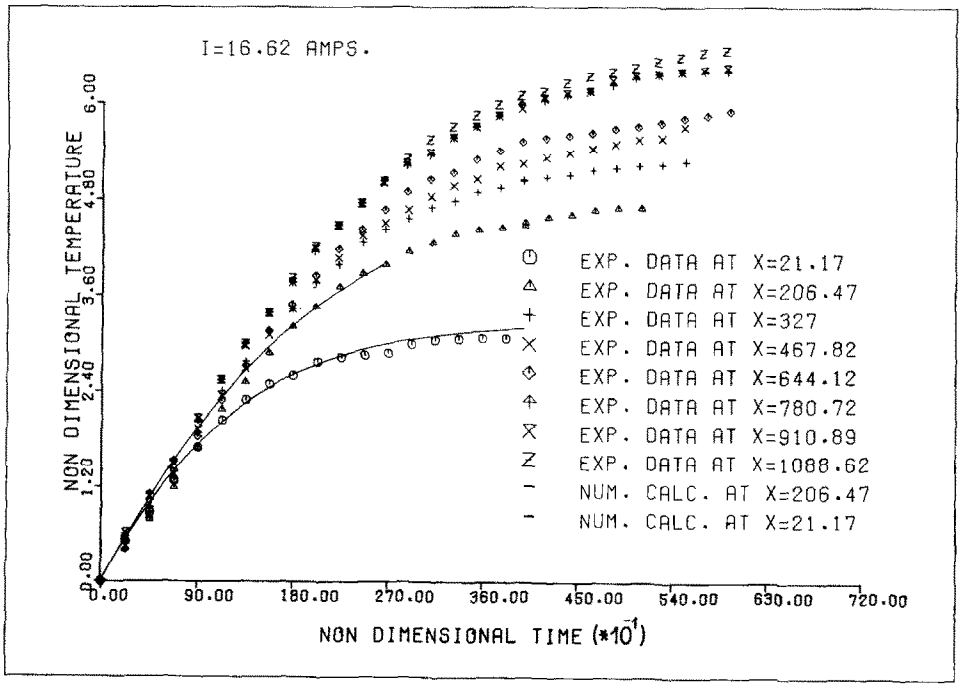

FIG. 2. Comparison of measured surface temperature response to finite difference calculations.

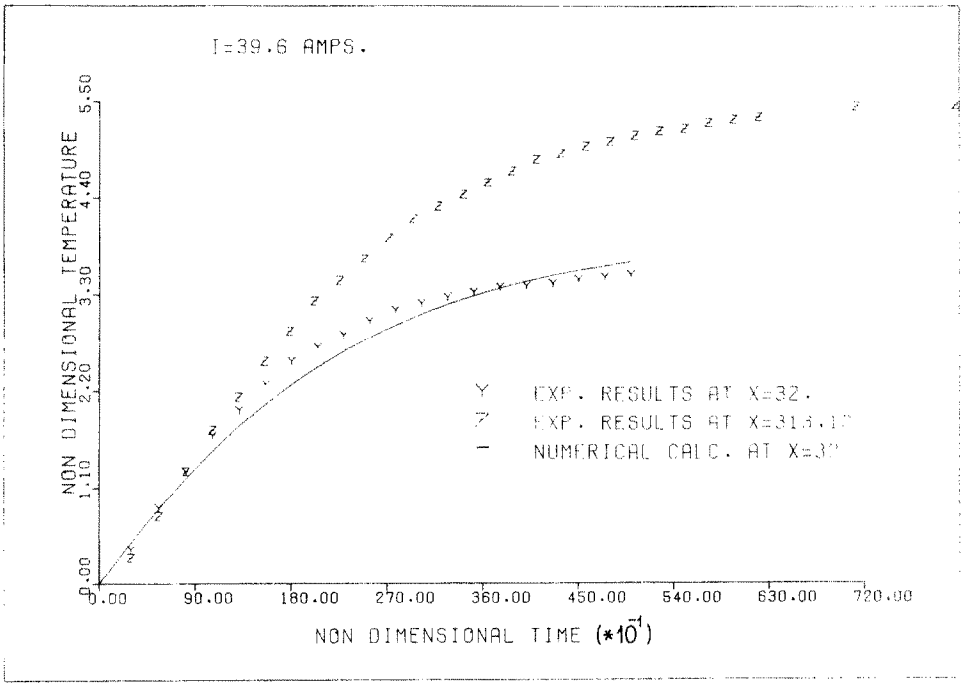

FIG. 3. Comparison of measured surface temperature response to finite difference calculations.

capacity of the composite plate was calculated to be 0.227 W-h/m^2 K. The plate was stretched vertically between two knife edges, and the whole assembly was supported by a stainless steel frame sitting in a 1.82 × 0.662 m × 1.83 m high stainless steel tank. The leading edge of the plate was 20 cm from the bottom of the tank. Eight, 127 μ copper–constantan thermocouples were placed along the vertical center line of the plate, imbedded in the Teflon layers. Four of the thermocouples were connected to a Beckman four-channel T511 Dynograph, the other four were connected to a Beckman T612. Thus, eight signals were recorded simultaneously.

The plate resistance was measured by connecting it in series with a precise resistor and passing a trickle current through, the voltage measured using a Hewlett Packard 3455A digital voltmeter gave the resistance. The plate assembly was heated by a Hewlett Packard 6475C DC power supply capable of supplying 0–110 V and 0–100 A. The current was initially loaded on a dummy load of the same resistance as that of the

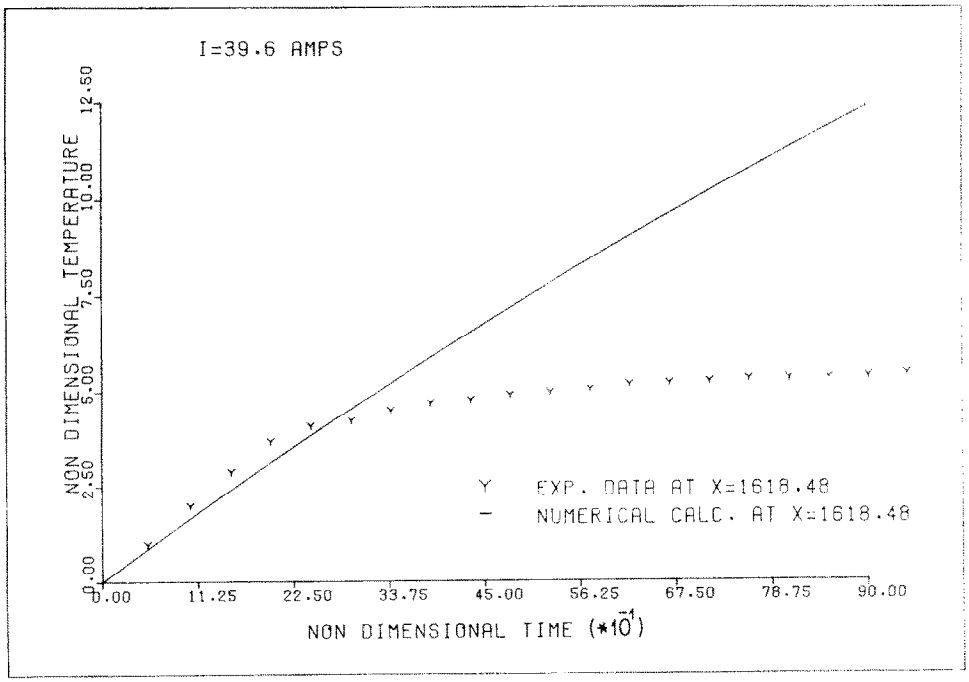

FIG. 4. Comparison of measured surface temperature response to finite difference calculations.

Table 1. Values of Q^* and transition parameters for different locations and flux levels

Current and heat flux	x-location (m)	Non-dim. X-location	Gr_x^*	G^*	X_{BT} (m)	X_{ET} (m)	Q^*	$(t_0 - t_\infty)_{ss}$ (°C)
8.59 A	0.0240	15.08	5.17×10^4	31.76	1.2164	1.6566	284.35	4.1
26.67 W/m^2	1.2410	779.96	3.7×10^{11}	746.16	1.2457	1.6987	283.77	8.9
16.62 A	0.0240	21.18	2.01×10^5	41.67	0.6535	0.7163	397.39	13.8
99.83 W/m^2	1.2410	1088.62	14.04×10^{11}	974.27	0.7038	0.7754	392.64	28.8
24.93 A	0.0240	25.64	4.32×10^5	48.56			480.65	27.0
224.6 W/m^2	1.2410	1323.68	30.69×10^{11}	1139.21			475.75	53.1
39.6 A	0.0240	32.00	10.49×10^5	57.99			597.11	58.6
566.7 W/m^2	1.2410	1618.48	68.61×10^{11}	1338.02			587.66	95.9

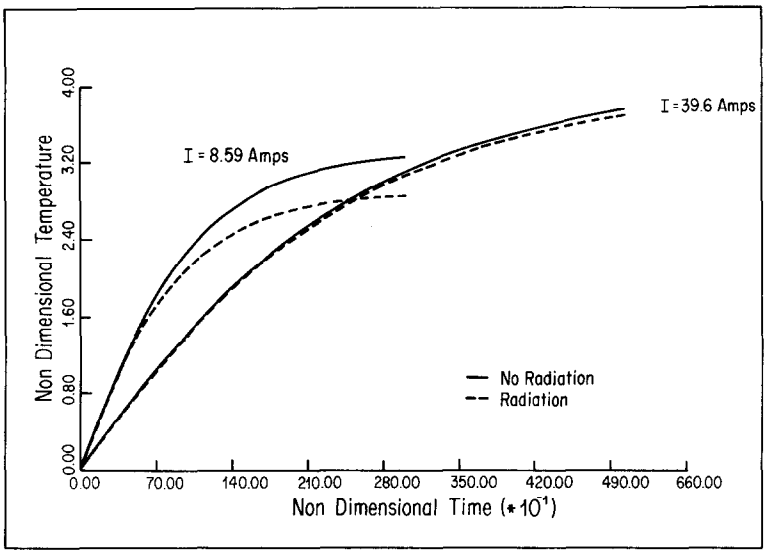

FIG. 5. Effect of thermal radiation on calculated surface temperature response.

plate assembly and then manually switched to the plate. Measurements were taken for four different levels of heat flux q'', ranging from 26.6 to 566.8 W/m^2. This resulted in temperature differences between the plate and ambient region ranging from 4.1 to 95.9°C, after steady state conditions were attained.

RESULTS AND CONCLUSIONS

In this experiment four different current levels, 8.59, 16.62, 24.93 and 39.6 A were used to take measurements. The non-dimensional thermal capacity parameter in equation (8), Q^*, varied from 284.81 to 597.11, for this range of current levels and downstream or x-locations. These values of Q^* were predicted in [1] to result in a quasi-static regime. The Biot number, $Bi = hs/k$, is calculated to be of the order of 0.02 for these experiments, which indicates a temperature gradient inside the plate of approximately 1% of $(t_0 - t_\infty)$.

Figures 1–3 show the measured transient surface temperature response downstream, in X, for each of the different current levels. Numerical calculations are shown for some of the different X-locations for comparison. Agreement between theory and experiment is quite good for most of the calculations. Part of the disagreement may be due to nonuniformity of plate thickness and surface conditions. The highest value of $(t_0 - t_\infty)_{ss}$ attained during the experiments was 95.9°C. The transient temperature response for the location at which that temperature difference is eventually attained is seen in Fig. 4. Transition to turbulence has clearly occurred early in the transient and the resulting turbulent transport reaches "steady state" much faster than for a laminar flow. However, the numerical solution is seen to be a good prediction during the early laminar part of the transient.

Mahajan and Gebhart reported the results of an experimental study [3], to determine the locations of the beginning and ending of the thermal transition region downstream, in steady flow. From these experiments, these locations, X_{BT} and X_{ET}, are calculated for different thermocouple and heat flux levels. These calculations indicate that several actual measurement locations are in the transition regime for a steady flow. One such measurement is seen in Table 1, at $x = 1.241$ m at 99.8 W/m^2. Nevertheless, some of these locations still show a laminar temperature response. The reason for the difference could be that the measurements in [3] were detected in the boundary layer. However, in this study, all thermocouples are in the plate assembly. Therefore, the effects of transition in the boundary layer first reach the plate thermocouples further downstream.

The effect of thermal radiation on the numerical solution of transport is seen in Fig. 5. Results of calculations are shown for two flux levels and at the same X-location. Radiation is seen to have a higher effect at lower flux levels. This is expected since convection increases more rapidly with temperature difference than does radiation, for small temperature differences.

REFERENCES

1. B. Sammakia and B. Gebhart, Transient and steady-state numerical solutions in natural convection, *Numer. Heat Transfer* **1**, 529–542 (1978).
2. B. Sammakia, A study of transient natural convection in air, M.S. Thesis, State University of New York at Buffalo, Buffalo, NY (1979).
3. R. L. Mahajan and B. Gebhart, An experimental determination of transition limits in a vertical natural convection flow adjacent to a surface, *J. Fluid Mech.* **91**, Part 1, 131–154 (1979).